CrossMark

Ablation morphology and ablation threshold of Ti-6Al-4V alloy during femtosecond laser processing

Niroj Maharjan[1,2] · Wei Zhou[1] · Yu Zhou[2] · Yingchun Guan[3]

Abstract

The research explores the use of femtosecond laser to clean the surface of Ti-6Al-4V alloy. The laser ablation threshold was determined from either depths or diameters of laser-induced craters. Both methods are expected to give the same results; however, it was found that ablation threshold can be determined more reliably from the diameters than from the depths. This can be understood from the study of the surface morphology. As the laser fluence increased, the ablated surface became increasingly rougher, making it difficult to measure the depths accurately. In contrast, diameters of laser-induced craters could be measured with much better certainty and thus enabled the ablation threshold to be determined more accurately. The ablation threshold was found to be 0.142 ± 0.010 J/cm^2 for 100 laser pulses at 130 fs pulse duration and 790 nm wavelength and it tends to decrease with increase in number of laser pulses. The single-pulse ablation threshold was determined to be 0.272 ± 0.021 J/cm^2.

1 Introduction

Laser cleaning has emerged as a credible alternative to conventional chemical-based processes in surface cleaning of aerospace components [1]. Lasers offer flexibility, high productivity and environment friendly operation that can be barely rivalled by any other processes. An effective cleaning requires complete removal of surface contaminants and damaged layer (in the range of μm to mm) while leaving the substrate unaffected.

Continuous wave and long pulse lasers ($> 10^{-6}$ s pulse duration) can clean the surface by selective evaporation of surface contaminants either by direct or indirect heat absorption [2]. However, there is a higher chance of excessive heating and damaging the substrate.

Short pulse lasers (10^{-6} to 10^{-9} s pulse duration), on the other hand, have proven to be a suitable tool for cleaning the surface under specific operating parameters [3]. They remove the contaminated surface layer by shock wave generation from rapidly expanding plasma. Nevertheless, the shock waves still pose a threat of damaging the substrate. In addition, the rise in surface temperature owing to the higher intensity levels (10^7–10^{10} W/cm^2) of short pulse laser might induce oxidation on the surface.

Recently, ultrashort pulse laser ($< 10^{-9}$ s pulse duration) has been used for cleaning and removing a thin damaged layer (in μm range) in aerospace components [4]. Compared to short pulse laser cleaning, the ultrashort pulses deposit energy more rapidly into the material and with time inadequate for thermalization of excited material, the ablation is clean and precisely defined. This can be advantageous for removal of exact damaged layer. However, even for these ultrashort pulses, some residual energy remains in the material which can produce thermal effects [5], although not as severe as in short pulse lasers. Thus, the surface morphology after ablation determines the effectiveness of the process and is greatly affected by the fluence used [6].

In this paper, we investigate the surface morphology after femtosecond laser ablation of Ti-6Al-4V alloy. Since cleaning requires near-threshold operation to prevent excessive damage to the substrate, a careful study of ablation threshold was performed using both ablation depth measurement

✉ Wei Zhou
wzhou@cantab.net

1 School of Mechanical and Aerospace Engineering, Nanyang Technological University, 50 Nanyang Avenue, Singapore 639798, Singapore

2 Advanced Remanufacturing and Technology Centre, 3 CleanTech Loop, Singapore 637143, Singapore

3 School of Mechanical Engineering and Automation, Beihang University, 37 Xueyuan Road, Beijing 100191, People's Republic of China

method and crater diameter measurement method. Furthermore, the reliability of obtained results is discussed, and the single-pulse ablation threshold is determined utilizing the incubation effect.

2 Experimental

The material used for all experiments was AMS 4911, Grade 5 titanium alloy (Ti-6Al-4V), which is commonly used in aircraft engine parts, airframe components and hydraulic systems. The microstructure of as-received Ti-6Al-4V after etching with Kroll's reagent (2% HF + 6% HCl + 92% H_2O) is shown in Fig. 1. The alloy was in annealed condition containing a uniform distribution of α phase and β phase. With the aim of studying the ablation morphology at near-ablation threshold operation, the sample surface was ground with progressively finer SiC papers (P180, P320, P400, P800, P1200) followed by polishing with 9 μ, 3 μ diamond suspensions and a final oxide polishing with 0.04 μ colloidal silica. The average surface roughness after polishing was measured to be about 44 nm. Before laser ablation, the sample was cleaned with alcohol, dried with an air gun and placed in a manually controlled X–Y translation stage of the experimental setup.

The ablation experiments were performed using the direct focusing technique with a commercially available titanium/sapphire laser (Quantronix Integra C1.0) in air. The laser emits 130 fs pulses of linearly polarized light at a central wavelength of 790 nm and with repetition rate of 1 kHz. Beam entrance diameter is 7 mm and approximates a Gaussian-shaped intensity distribution at the center. The sample was placed at the focal plane of the focusing lens (focal length $f = 100$ mm). The vertically polarized laser beam was
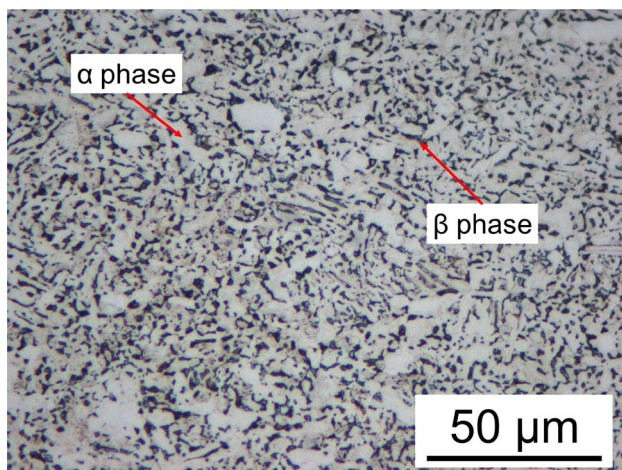
Fig. 1 Microstructure of as-received Ti-6Al-4V showing uniform distribution of α and β phases

directed perpendicularly onto the sample surface. The number of pulses striking the surface was controlled by means of a computer-controller fast optical shutter. The pulse energy was varied using a combination of energy attenuators and optical filters (Edmund Optics) placed in the path of beam travel and measured using a power meter (Coherent Inc.) just after the objective lens. The power meter was used together with the manufacturer's software, which enabled laser power to be measured in real time.

The laser irradiated on the surface was controlled using computer software (CyberLase) and a series of surface craters were created at different pulse energies at a constant number of pulses. At least three holes were produced at each value of laser fluence and an average value was calculated. All depth measurements were performed using a confocal microscope (Carl Zeiss Smartproof5) and surface crater diameters were measured using images from a scanning electron microscope (JEOL 5600LV).

3 Results and discussion

3.1 Morphological results

The evolution of damage crater on the sample surface with increase in laser fluence is shown in Fig. 2. No significant damage was observed at fluence below 0.250 J/cm^2. A small surface crater formed at fluence of 0.250 J/cm^2 as shown in Fig. 2a with ripple patterns in the ablated area. These ripples were oriented perpendicular to the polarization direction of laser beam and had periodicity of the order of laser wavelength. They are thought to form from the near-field interference of incident laser beam and surface plasmons being excited in the air and metal interface [7, 8]. Since no evidence was present to suggest surface melting during ripple formation, the material removal is considered to occur basically by direct vaporization from absorption of laser energy.

The size of ablated area increased with increase in laser fluence (see Fig. 2). This is expected since the laser beam has Gaussian shaped intensity profile and at higher fluence, more area of the intensity profile will be above ablation threshold. At fluences greater than 1.127 J/cm^2, a strong ablation regime developed at the center of the crater. The strong ablation regime had ripple-like appearance at the center with ripple periodicity in micrometer range and oriented perpendicular to original nano-ripples (Fig. 2d). However, the ripple pattern quickly disappeared with increase in fluence and rough bumps formed at the center. At very high fluence (> 1.500 J/cm^2), the resulting morphology appeared like in Fig. 2f with a deep hole at the center and a re-solidified area around the hole.
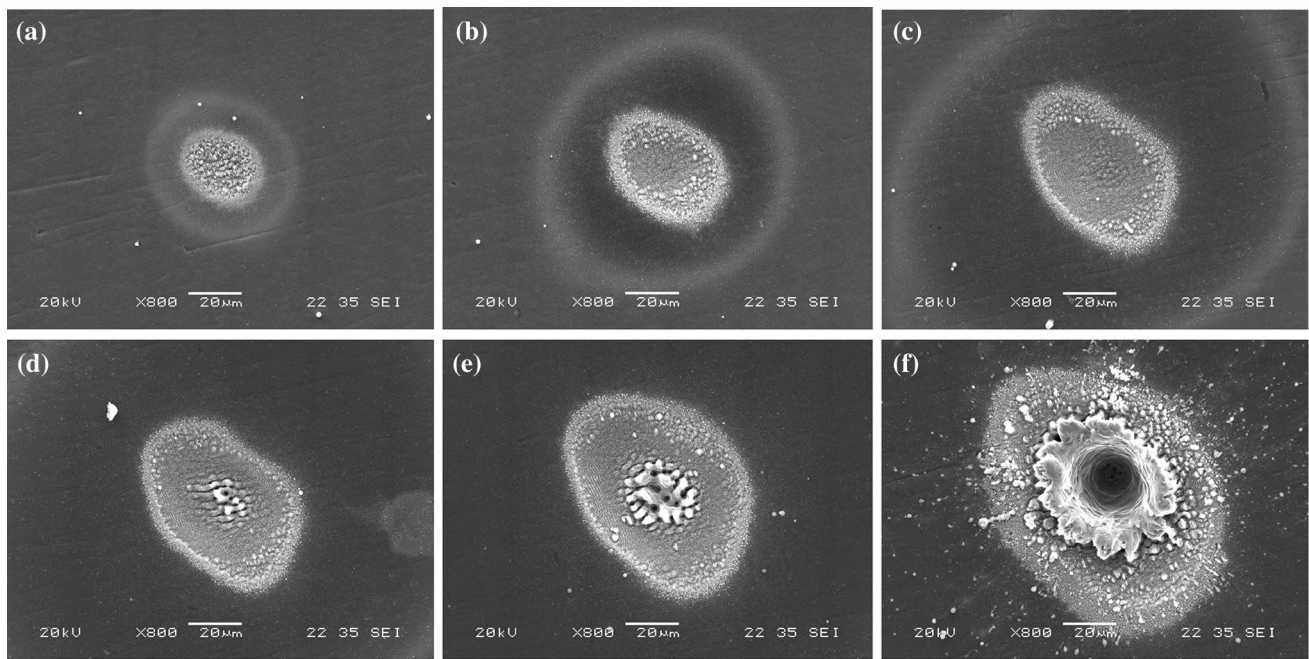
Fig. 2 SEM images showing morphological evolution of Ti-6Al-4V surface after irradiation with 100 shots and fluence of **a** 0.250 J/cm^2, **b** 0.387 J/cm^2, **c** 0.765 J/cm^2, **d** 1.127 J/cm^2, **e** 1.851 J/cm^2, and **f** 7.896 J/cm^2

The ultrashort pulse laser metal ablation is generally believed to occur by energy transfer from photon to electrons and then to lattices. However, the exact mechanism may vary depending on difference in laser pulse duration, laser fluence and material properties [9]. The ablation at lower fluences is considered to occur by spallation (see Fig. 3) [10]. At low fluence regime, the volume expansion of the irradiated surface changes the internal pressure in the solid material. When tensile stress exceeds the tensile strength limit of the material, fractures parallel to the surface of the solid appear. These fractures initially generate as micro-pores just beneath the surface before coalescing to result in ejection of the topmost surface layer. Studies suggest that spallation occurs at fluences close to ablation threshold [11].

At higher fluences, the higher heating rate quickly heats the material above its equilibrium boiling temperature. The superheating causes molten layer to enter meta-stable phase with variation in density and specific heat [6]. This forms a homogeneous nucleation of vapor nuclei in regions of low density (see Fig. 4). The upward movement of these vapor bubbles results in rapid phase explosion of the material expelling a mixture of vapor and metal droplets away from the center [12]. The rapid cooling and solidification forms the final structure as seen in Fig. 2f.

In order to study the effect of number of pulses on ablation, series of damage craters were created at a constant fluence. The number of pulses were varied from 5 to 1000. It was observed that increasing the number of pulses resulted in an increase in ablation depth (see Figs. 5, 6). However, the number of pulses had a negligible effect on the ablation diameter at the surface (see Fig. 6). Another interesting thing observed was that at
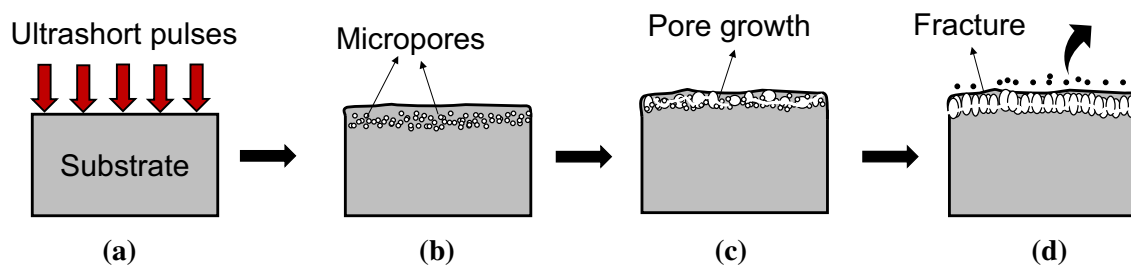

Fig. 3 Illustration showing ablation by spallation at low fluences—**a** laser irradiation, **b** formation of micropores due to volume expansion, **c** pore coalescence, and **d** fracture and material removal
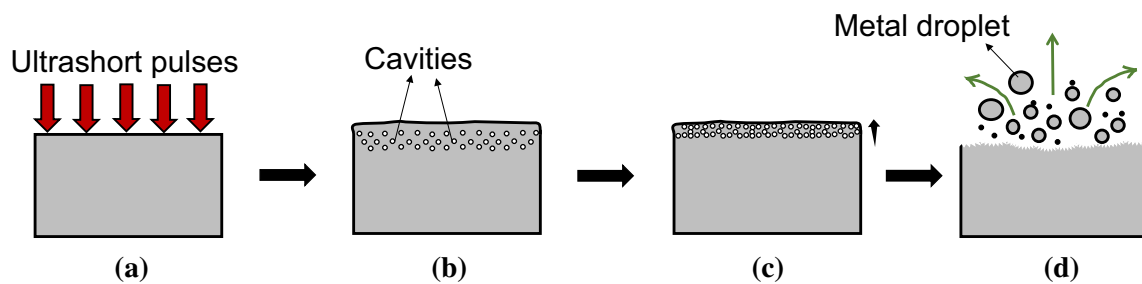
Fig. 4 Illustration showing ablation by phase explosion at high fluences—**a** laser irradiation, **b** formation of cavities in low density region, **c** upward movement of cavities, and **d** metal droplets and vapor expulsion
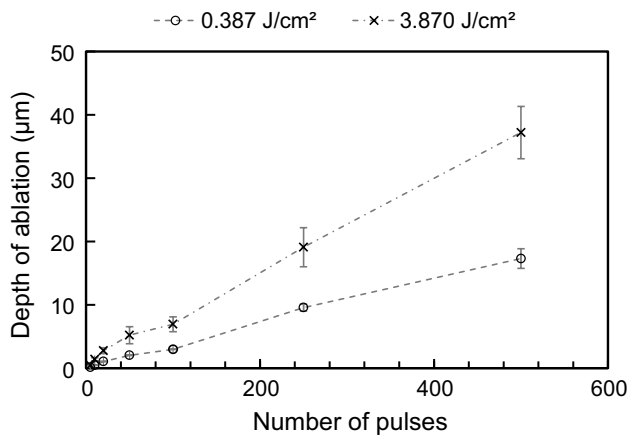

Fig. 5 Graph showing increase in ablation depth with increase in number of pulses. Note that a higher error occurs at larger ablation depth due to limitation of the confocal microscope used for measurement. The depth at 1000 shots could not be measured

3.2 Ablation threshold calculations

The ablation threshold of a material is an important parameter that determines the damage to the substrate during laser-material interaction. Operating the laser at lower fluences near ablation threshold produces minimal damage to the substrate as seen in Sect. 3.1. The determination of exact ablation threshold would be helpful in choosing the proper parameters for femtosecond laser cleaning. However, most studies use pure metals to determine ablation threshold [6, 14–16]. Mannion et al. [17] studied the ablation morphology of pure titanium using a femtosecond laser (wavelength 775 nm, pulse duration time 150 fs and repetition rate 100 Hz) and measured ablation threshold of pure titanium to be about 0.1021 J/cm^2 for 100 pulses. Hasida et al. [14] used short pulses of 800 nm and 40 fs to study multishot ablation of pure titanium and obtained threshold fluence of about 0.074 J/cm^2. Similarly, other studies on ultrashort pulsed laser ablation of pure titanium found threshold fluence values ranging from 0.050 J/cm^2 [15] to 0.081 J/cm^2 [16].

It is understandable that using a pure metal eliminates the effect of material inhomogeneity and helps to emphasize in investigating the interplay between multiple processes initiated by laser action on the metal surface. In real applications, however, pure metals are rarely used and ablation threshold for alloys must be determined. Turner et al. [2] calculated ablation threshold of titanium alloy to be about 0.708 J/cm^2 and 0.450 J/cm^2 for pulsed Nd:YAG (wavelength 1064 nm, repetition rate 1–30 kHz pulse width 100 ns) and excimer laser (wavelength 248 nm, repetition rate 1–100 Hz, pulse width 12–14 ns) respectively. Zheng et al. [18] used picosecond laser (wavelength 1064 nm, repetition rate 10 kHz, pulse width 10 ps) to investigate the ablation of titanium alloy and calculated it to be about 0.109 J/cm^2 for 2000 pulses. However, they only considered one ablation condition to calculate the ablation threshold. A different ablation threshold can result just by changing the experimental parameters such as wavelength and pulse duration [19]. Moreover, the ablation threshold for Ti-6Al-4V alloy during femtosecond laser ablation was not found in the literature. Therefore, an exact

lower fluences (< 1 J/cm^2), the strong ablation regime did not appear even after increasing the number of pulses. Contrary to this, a flat surface melting was observed at high fluences at number of shots as low as 5.

The results suggest that the ablated surface has rough morphology at higher fluences and the rough ablation structure depends on the fluence rather than on the number of pulses. At lower fluence, most of the laser energy is utilized to directly ablate the surface. However, at higher fluence, the surplus energy after ablating the material results in melting at the center. According to Vorobyev and Guo [13], some residual thermal energy is deposited in the material even at lower fluences due to laser induced surface modification, exothermic chemical processes and gas pressure effects. However, such residual heating is not enough to melt the surface at lower fluences. The ablation depth increases with increase in pulse number for both cases due to reduction in ablation threshold due to incubation effect [6] (discussed further in Sect. 3.3).

ablation threshold for Ti-6Al-4V alloy is determined in this section. Both ablation depth measurement [20] and surface damage diameter measurement [21], which are the two most commonly accepted methods for quantification of ablation damage, are utilized for determination of ablation threshold.

3.2.1 Ablation depth measurement

The ablation of a material during ultrashort pulsed laser irradiation can be detected by observing if there is plasma formation during the laser-material interaction. It is possible to determine the ablation threshold of a material by studying the ablation rate or depth removed per pulse, L. The relation between ablation rate, L, and peak fluence, ϕ_0, for a fixed number of pulses is given by [20]:

$$L = \alpha^{-1}\ln\left(\frac{\phi_0}{\phi_{th}}\right) \tag{1}$$

where ϕ_{th} is the ablation threshold of the material and α^{-1} is the effective heat penetration depth which measures the distance through which the heat energy is diffused via electrons.

It is noteworthy to mention that peak fluence was chosen here rather than average fluence for threshold calculations. This is mainly because of the bell-shaped intensity profile of Gaussian beam. In a Gaussian beam, the energy will be maximum at the center and decrease towards the edge. Thus, when the fluence value is comparable to ablation threshold, only the energy above threshold value would cause ablation. Thus, peak fluence gives a more meaningful estimation of ablation fluence than average fluence.

The peak fluence of the Gaussian beam is given by:

$$\phi_0 = \frac{2E_p}{\pi\omega_0^2} \tag{2}$$

where E_P is the pulse energy and ω_0 is the laser beam spot radius at $1/e^2$ intensity. The spot radius was calculated to be 27.54 μm according to [22] and peak fluences were calculated for different pulse energies accordingly. Since the ablation rate is proportional to the logarithm of peak fluence, the ablation threshold can be calculated by finding the value of fluence for zero ablation rate, i.e. $L = 0$.

The graph of ablation rate versus peak fluence for 100 laser pulses is shown in the Fig. 7. The ablation rate is calculated by dividing the ablation depth by number of pulses i.e. 100. The effective heat penetration depth and the ablation threshold are calculated by fitting (1) to the graph. From the fitting, the effective heat penetration depth and ablation threshold are calculated to be 26.36 ± 2.35 nm and 0.150 ± 0.029 J/cm^2.

It is clear from Fig. 7 that the goodness of fit is not so accurate as represented by R^2 value. This can be attributed to the measurement method and the rough ablation morphology obtained due to interaction of laser with inhomogeneous material. The depth measurements were performed using confocal microscopy. Since the ablation holes were narrow (in micrometer range at the surface) and the depth of ablation was quite deep (tens of microns for multishot ablation), the measured depth values were prone to high degree of uncertainly due to instrument limitation (see Fig. 8). In addition to this, the non-uniform depth profile and the formation of rough re-melted region at the ablation center at higher fluences (see Fig. 2d–f) pose a great challenge in accurate ablation depth measurement. Therefore, there was a lot of scattering and the calculated threshold value may not represent the accurate value. It was thus deemed necessary to use another method that is more robust for accurate ablation threshold calculation. Measurement of crater diameter formed due to ablation can be a good alternative and has been applied by several researchers to calculate ablation threshold of a material.

3.2.2 Crater diameter measurements

When a material is irradiated with a laser having Gaussian spatial intensity beam profile, a simple relation exists between the crater diameter, D, and peak fluence of the beam, ϕ_0, which is given by [21]:

$$D^2 = 2\omega_0^2 \ln\frac{\phi_0}{\phi_{th}} \tag{3}$$

Since the peak fluence, ϕ_0, is linearly dependent on pulse energy as shown in (2), the beam spot radius, ω_0, can be calculated from a plot of square of crater diameters, D^2, and the logarithm of the laser pulse energy, E_p. From our calculations, the average beam spot radius was found to be 27.82 ± 0.88 μm, where the error was calculated from the error values associated with the squared diameters. This value is almost same to the value obtained using [22] and hence, was used for rest of the experiments.

After determining the beam spot radius, the ablation threshold, ϕ_{th}, can be determined from (3) by plotting a graph of squared diameter, D^2, against the peak fluence values. Due to the beam divergence during propagation, the laser spot shape is not perfectly circular, but is elliptical (Figs. 2, 6). Therefore, the crater diameter was calculated assuming the area of ellipse to be equal to area of equivalent circle with effective diameter D. Afterwards, the ablation threshold is measured by extrapolating D^2 back to zero. Using this method, the ablation threshold value for 100 shots was determined to be 0.142 ± 0.010 J/cm^2, which is close to the value calculated using ablation depth measurements.
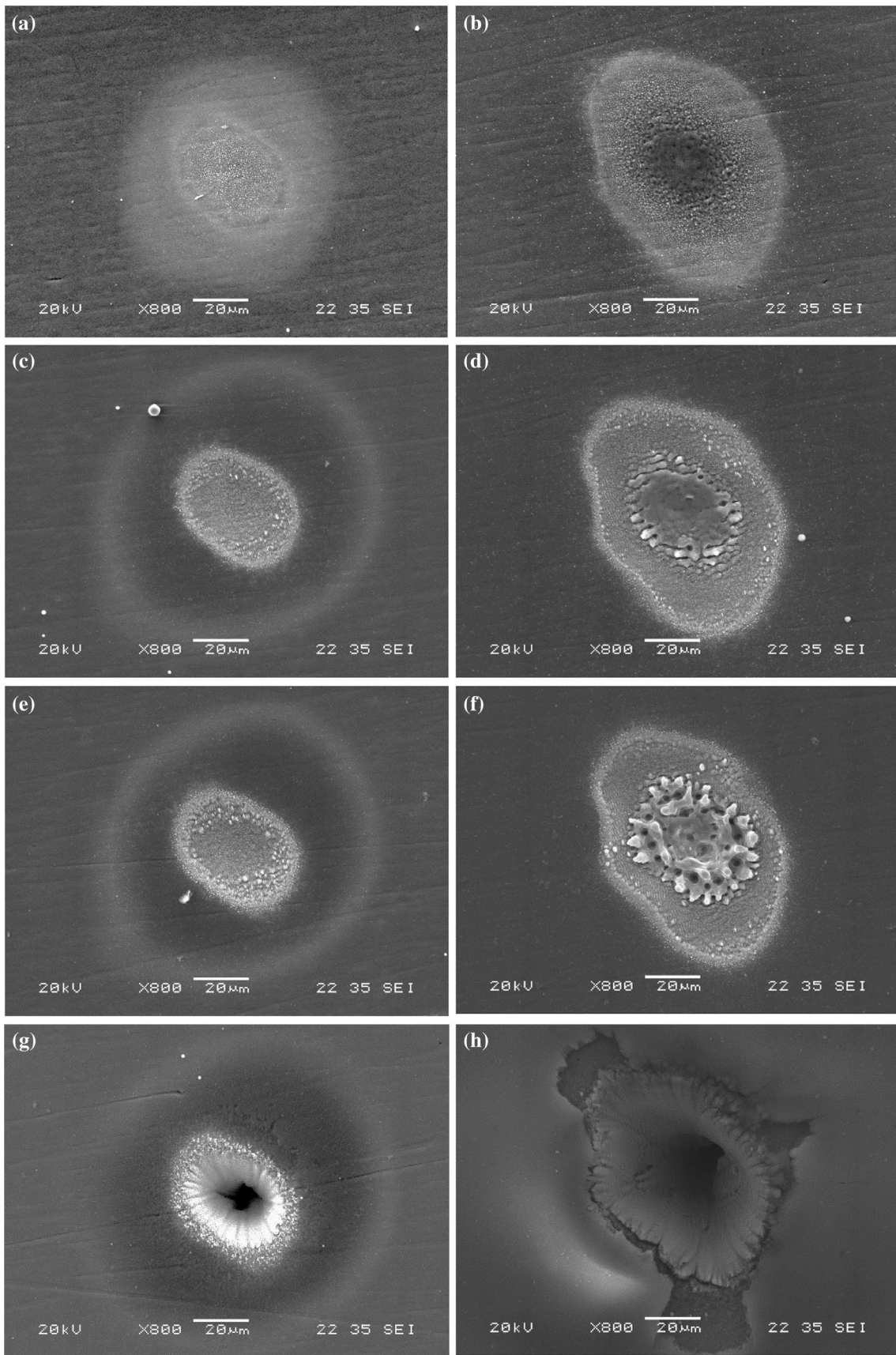
SEM images showing evolution of ablation damage with increasing number of pulses for constant fluence of 0.387 J/cm^2 (**a, c, e, g**) and 3.870 J/cm^2 (**b, d, f, h**): **a, b** 5 shots; **c, d** 50 shots; **e, f** 100 shots; and **g, h** 1000 shots

The ablation threshold calculated by this method is more accurate than the value calculated by depth measurement method. As can be seen in Fig. 9, there is a less scattering of measured diameters. The squared diameter and peak fluence also show a good correlation as indicated by R^2 value. The error in ablation threshold was found to be 0.010 J/cm^2 which suggests that this method is more reliable than ablation depth measurement method.

3.3 Incubation effect

Following the crater diameter measurement method mentioned in Sect. 3.2, the ablation threshold value for different number of pulses were calculated. The results are plotted in graph of ablation threshold versus number of pulses as shown in Fig. 10. The value of ablation threshold decreased with increase in number of pulses due to incubation effects. Clearly the multishot ablation threshold is lower than single-pulse ablation indicating that the damage can occur at lower fluence values when the number of pulses is increased. Different theories are available in the literature on the mechanism responsible for incubation [23–25]. During multishot ablation, the reflectance drops drastically after the first few laser shots. Therefore, a higher percentage of incident energy is absorbed by the material which results in higher ablation rate. On the other hand, the excitation of surface plasmons could also aid in energy coupling mechanism. The overall outcome is the reduction in the ablation threshold value. It is, however, important to note that the ablation threshold does not keep on decreasing and stabilizes after about 500 shots. This is because of the reduction in beneficial effect of reflectance drop after few pulses and decoupling of plasma from the surface.

The incubation effect can be quantitatively analyzed using the power law equation by [26], which is given as:

$$\phi_{th}(N) = \phi_{th}(1)N^{S-1} \tag{4}$$

where $\phi_{th}(N)$ is the ablation threshold for N laser pulses, $\phi_{th}(1)$ is the single-pulse ablation threshold, N is the number of laser pulses and S is the incubation coefficient. When $S = 1$, there is no incubation effect. Equation (4) can be rearranged as:

$$N\phi_{th}(N) = \phi_{th}(1)N^{S} \tag{5}$$

By plotting a graph of $N\phi_{th}(N)$ versus number of pulses and fitting a least square curve, the single-pulse ablation threshold and incubation coefficient can be determined (see Fig. 11). For Ti-6Al-4V, it was found to be $\phi_{th}(1)$

$= 0.272 \pm 0.021$ J/cm^2 and $S = 0.855 \pm 0.014$. The calculated value is very close to the single-shot ablation threshold of 0.28 ± 0.02 J/cm^2 for pure titanium mentioned in the literature [6].

In order to verify the accuracy of the values obtained, further ablation experiments were carried out at values close to the ablation threshold. Ablation was assumed to occur if there was plasma formation during the interaction. Since it was difficult to quantify the topographical changes brought about by a single pulse, a constant laser pulse of 5 shots was used. This, not only produced appreciable change on the surface, but also aided in operating the laser at values close to ablation threshold ($\phi_{th}(5) = 0.215$ J/cm^2). As expected, no plasma was detected at fluences below or near the ablation threshold. On increasing the laser fluence, a faint plasma appeared when the laser was operated at the fluence of 0.288 J/cm^2. Investigation of surface topography showed the removal of material and surface ripples in the laser-irradiated area (see Fig. 12). Even though the fluence, which was exactly the same as the ablation threshold, could not be used due to the limitation of the laser system, the obtain results still validate the correctness of calculated threshold values.

4 Conclusions

A detailed study of ablation on Ti-6Al-4V alloy surface irradiated with femtosecond laser (wavelength 790 nm, pulse width 130 fs, repetition rate 1000 Hz) has been performed. The ablation threshold was calculated using both depths method and diameters method. The following conclusions can be derived from the results:
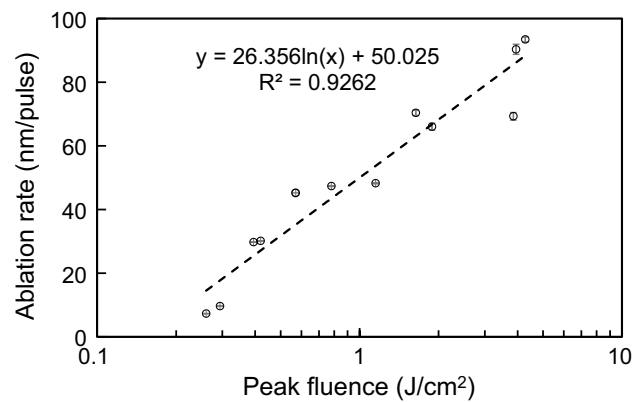

Fig. 7 Graph of ablation rate of Ti-6Al-4V against peak fluence when ablated with femtosecond laser (wavelength 790 nm, pulse width 130 fs) for constant 100 laser shots. The error bars and the size of data markers approximate the error on crater diameters and fluence values, respectively. The line represents the least squares fit according to (1) and R^2 value represents the goodness of fit

Fig. 8 3D view and 2D profile of Ti-6Al-4V surface ablated with a pulse energy of 19.5 μJ and 100 shots. Note that due a steep slope and rough morphology at the ablation center and periphery, the data points could not be measured
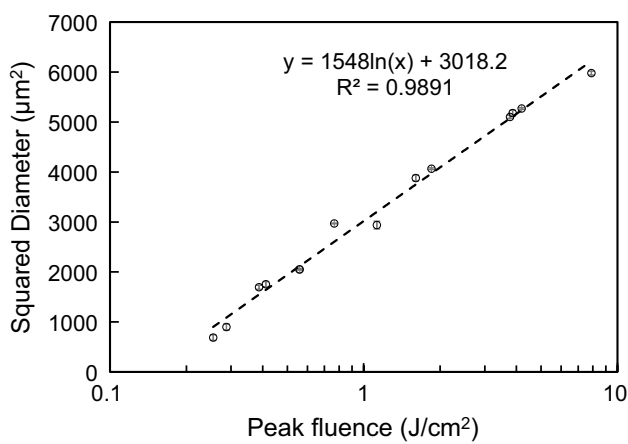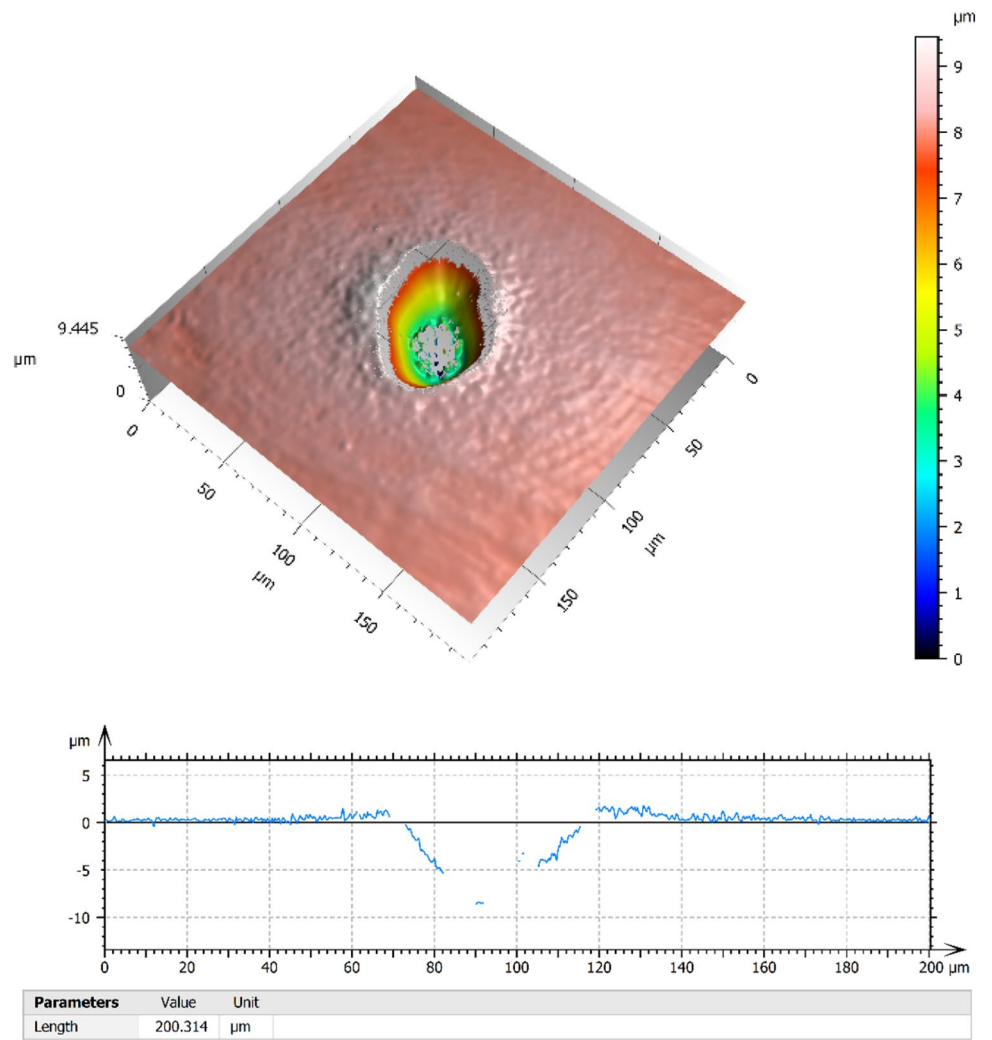

Parameters	Value	Unit
Length	200.314	μm

Fig. 9 Graph of squared diameter, D^2, of ablated craters in Ti-6Al-4V as a function of peak fluence at 100 laser shots. The line represents the least-squares fit according to (3)
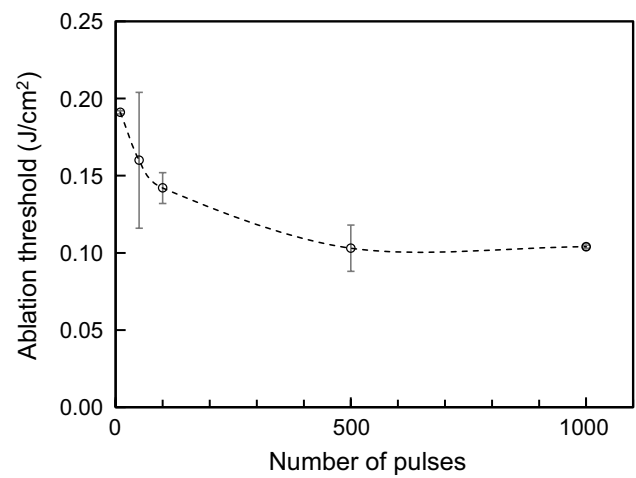
$$y = 1548\ln(x) + 3018.2$$
$$R^2 = 0.9891$$

Fig. 10 Graph showing the reduction in ablation threshold with increase in number of pulses
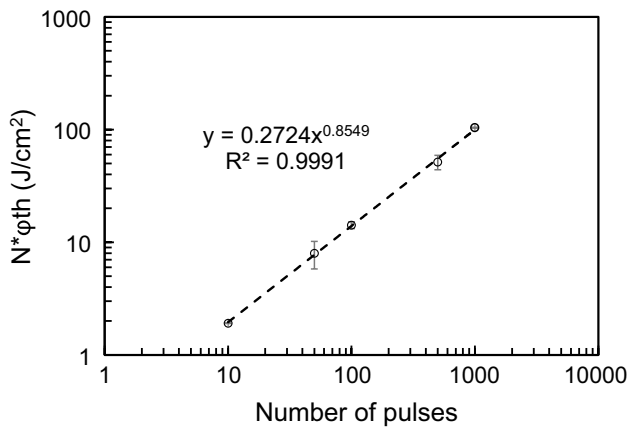
Fig. 11 Graph of accumulation fluence against number of pulses; the line represents the least square fit according to (5)

- Femtosecond laser processing of a material at near-ablation threshold produces a smooth surface ablation quality, which is desirable for various surface engineering applications like drilling, texturing and cleaning.

- Increasing the laser fluence increases crater diameter since more area of Gaussian intensity profile will fall above ablation threshold. Increasing number of laser shots resulted in increase of ablation depth though.

- Based on the depth measurement method, the multishot ablation threshold for Ti-6Al-4V alloy irradiated with femtosecond laser of 130 fs pulse duration and 790 nm wavelength at 100 laser shots was found to be 0.150 ± 0.029 J/cm^2. It was calculated to be 0.142 ± 0.010 J/cm^2 using crater diameter measurement method. Since there was a high degree of uncertainty in depth measurements than diameter measurements, the ablation threshold value obtained using diameter method is considered more reliable.

- Ablation threshold was found to decrease with increase in number of pulses due to damage accumulation effect. The single-pulse ablation threshold was calculated to be 0.272 ± 0.021 J/cm^2. The laser must be operated slightly above the ablation threshold value to remove the damaged layer (in the range of 1–5 μm) on the surface with minimal damage to the substrate.
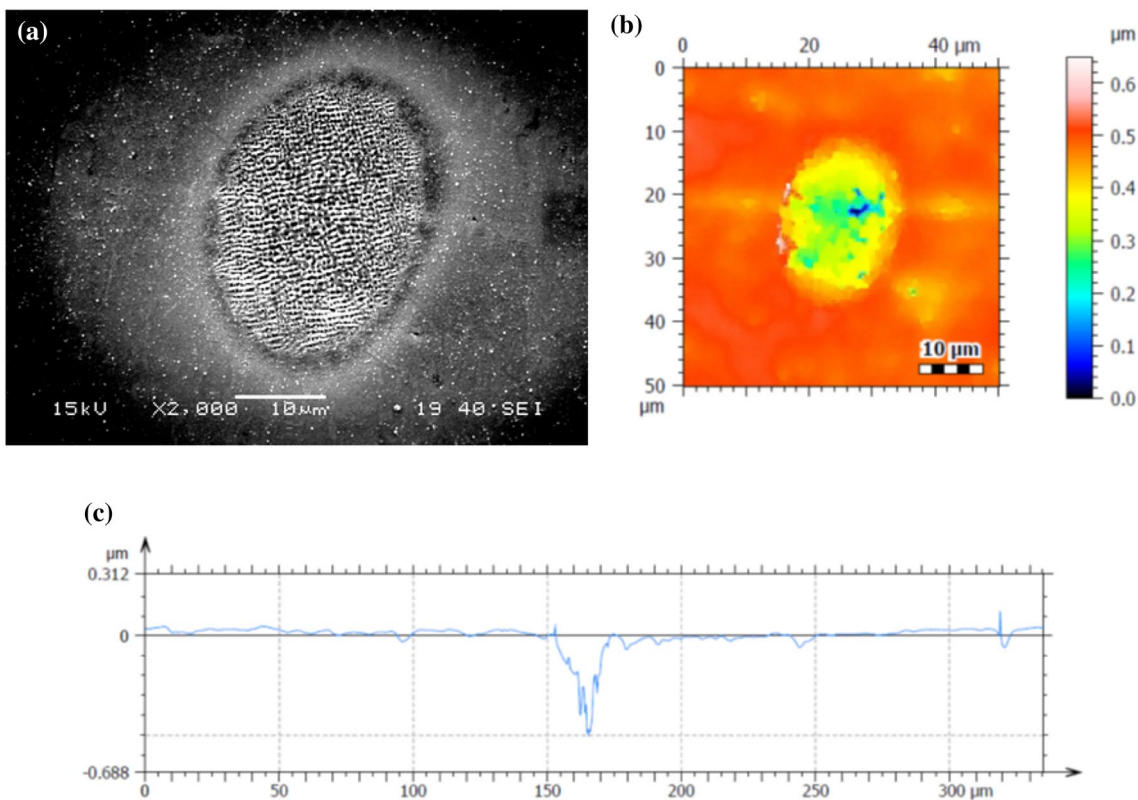

Fig. 12 Ablation morphology at 0.288 J/cm^2 which is slightly higher than ablation threshold of 0.215 J/cm^2 for 5 laser pulses, **a** SEM micrograph showing ablated surface, **b** surface topology, and **c** line profile across the ablated surface showing ablation depth of about 0.5 μm

References

1. D.J. Whitehead, P.L. Crouse, M.J.J. Schmidt, L. Li, M.W. Turner, A.J.E. Smith, Appl. Phys. A **93**, 123 (2008)
2. M.W. Turner, P.L. Crouse, L. Li, Appl. Surf. Sci. **252**, 4792 (2006)
3. M.W. Turner, P.L. Crouse, L. Li, Appl. Surf. Sci. **253**, 7992 (2007)
4. N. Maharjan, W. Zhou, Y. Zhou, Y.C. Guan, *Conference on Lasers Electro-Optics Pacific Rim* (IEEE, Singapore, 2017)
5. Y. Hirayama, M. Obara, Appl. Surf. Sci. **197**, 741 (2002)
6. P.T. Mannion, J. Magee, E. Coyne, G.M. O'connor, T.J. Glynn, Appl. Surf. Sci. **233**, 275 (2004)
7. J. Bonse, A. Rosenfeld, J. Laser Appl. **042006**, 1 (2012)
8. J. Bonse, R. Koter, M. Hartelt, D. Spaltmann, S. Pentzien, S. Höhm, A. Rosenfeld, J. Krüger, Appl. Phys. A **117**, 103 (2014)
9. S.I. Anisimov, B.L. Kapeliovich, T.L. Perelman, Zh. Eksp. Teor. Fiz. **66**, 776 (1974)
10. J. Cheng, C.S. Liu, S. Shang, D. Liu, W. Perrie, G. Dearden, K. Watkins, Opt. Laser Technol. **46**, 88 (2013)
11. D. Perez, L.J. Lewis, Phys. Rev. B **67**, 184102 (2003)
12. R. Kelly, A. Miotello, Phys. Rev. E **60**, 2616 (1999)
13. A.Y. Vorobyev, C. Guo, Appl. Phys. Lett. **86**, 11916 (2005)
14. M. Hashida, Y. Miyasaka, T. Nishii, M. Shimizu, S. Inoue, S. Sakabe, Electron. Commun. Jpn **99**, 88 (2016)
15. M. Ye, C.P. Grigoropoulos, J. Appl. Phys. **89**, 5183 (2001)
16. L. Gemini, M. Hashida, Y. Miyasaka, S. Inoue, J. Limpouch, T. Mocek, S. Sakabe, Appl. Surf. Sci. **336**, 349 (2015)
17. P. Mannion, J. Magee, E. Coyne, G.M. O'Connor, in *Opto Irel*. (International Society for Optics and Photonics, Bellingham, 2003), pp. 470–478
18. B. Zheng, G. Jiang, W. Wang, K. Wang, X. Mei, AIP Adv. **4**, 31310 (2014)
19. M.S. Brown, C.B. Arnold, Laser Precis. Microfabr. **135**, 91 (2010)
20. S. Nolte, C. Momma, H. Jacobs, A. Tünnermann, B.N. Chichkov, B. Wellegehausen, H. Welling, JOSA B **14**, 2716 (1997)
21. J. Bonse, J.M. Wrobel, J. Krüger, W. Kautek, Appl. Phys. A Mater. Sci. Process. **72**, 89 (2001)
22. W.M. Steen, in *Laser Material Processing*, Third (Springer, New York, 2003)
23. J. Byskov-Nielsen, J.-M. Savolainen, M.S. Christensen, P. Balling, Appl. Phys. A Mater. Sci. Process. **101**, 97 (2010)
24. D. Perez, L.J. Lewis, Phys. Rev. Lett. **89**, 255504 (2002)
25. N.M. Bulgakova, I.M. Bourakov, Appl. Surf. Sci. **197**, 41 (2002)
26. Y. Jee, M.F. Becker, R.M. Walser, JOSA B **5**, 648 (1988)